



CHORUS

This is the accepted manuscript made available via CHORUS. The article has been published as:

Charge-Induced Saffman-Taylor Instabilities in Toroidal Droplets

A. A. Fragkopoulos, A. Aizenman, and A. Fernández-Nieves

Phys. Rev. Lett. **118**, 264501 — Published 26 June 2017

DOI: [10.1103/PhysRevLett.118.264501](https://doi.org/10.1103/PhysRevLett.118.264501)

Charge-Induced Saffman-Taylor Instabilities in Toroidal Droplets

A. A. Fragkopoulos,¹ A. Aizenman,¹ and A. Fernández-Nieves¹

¹*School of Physics, Georgia Institute of Technology, Atlanta, Georgia 30332-0430, USA*

(Dated: May 15, 2017)

We show that charged toroidal droplets can develop finger-like structures as they expand due to Saffman-Taylor instabilities. While these are commonly observed in quasi-two dimensional geometries when a fluid displaces another fluid of higher viscosity, we show that the toroidal confinement breaks the symmetry of the problem, effectively making it quasi-two dimensional and enabling the instability to develop in this three dimensional situation. We control the expansion speed of the torus with the imposed electric stress and show that fingers are observed provided the characteristic time scale associated to this instability is smaller than the characteristic time scale associated to Rayleigh-Plateau break-up. We confirm our interpretation of the results by showing that the number of fingers is consistent with expectations from linear stability analysis in radial Hele-Shaw cells.

Droplets are spherical since the sphere minimizes the area for a given volume [1]. In the presence of charge, however, the balance between surface tension and electric stresses results in an ellipsoidal shape [2]. With even more charge, the elongated droplet eventually becomes unstable and develops conical points at the ends that evolve into charged jets, which ultimately break into small drops [2]. For a charged toroidal droplet the situation is markedly different. In this case, the surface charge density is not constant throughout the surface; it is smallest in the inside of the torus, where the polar angle θ [see Fig. 1(a)], is zero, and it is largest in the outside of the torus, where $\theta = \pi$. This breaks the axisymmetry of the cylinder and causes the toroidal droplet to expand with velocity \vec{U}_o [see Fig. 1(a)], before break-up occurs due to Rayleigh-Plateau instabilities [3]. Note, however, that due to the symmetry breaking in the problem, the expansion becomes an essentially two-dimensional problem.

In this Letter, we show that charged toroidal droplets can evolve via the Saffman-Taylor instability [4], which occurs when a fluid displaces another fluid of higher viscosity in a confined quasi-two dimensional flow [5]. Typically, the displacement of the high-viscosity fluid is driven by continuous pumping of the low-viscosity fluid in a Hele-Shaw cell, which consists of two parallel plates a small distance away from each other [4]. The interface between the two fluids moves at a certain speed before destabilizing and resulting in the formation of fingers. In our experiments, the expansion speed, which results from the particular surface charge distribution on the torus, is controlled by the applied voltage. By varying this speed, we demonstrate that the Saffman-Taylor instability competes with Rayleigh-Plateau break-up, and that the faster of the two determines the fate of the toroidal droplet. We further confirm that our observations are indeed due to viscous fingering by showing that the number of fingers determined experimentally is consistent with what is expected from linear stability analysis in radial Hele-Shaw cells.

We generate charged toroidal droplets by injecting a low-viscosity liquid inside a high-viscosity liquid that is contained inside a glass cuvette, which is placed on top of a metallic rotating stage [3]. The injection is through a metallic needle offset from the center of rotation of the cuvette [6], as

schematically shown in Fig. 1(b). As a result of the imposed rotation, a curved jet forms, eventually closing onto itself and resulting in the generation of a toroidal droplet. The typical liquid pumped is within 20 and 40 μL . Note that by controlling the distance between the needle and the rotation axis, as well as the total volume we pump, we can independently vary the tube radius, a_0 , and the radius of the central circle radius, R_0 [Fig. 1(a)]. We then apply a voltage difference across the metallic needle and the rotating stage [Fig. 1(b)], and monitor the evolution of the toroidal droplet by imaging from below using a CCD camera. We emphasize that the experiments are performed with the metallic needle inside the torus. Therefore, the torus is always equipotential and the experiments are performed at constant voltage, V . The low-viscosity liquid is water containing 16 mM of sodium dodecyl sulfate (SDS); its dynamic viscosity is $\mu_1 = 1 \text{ mPa} \cdot \text{s}$. The high-viscosity liquid is a mixture of a 65 cSt aminopropyl terminated silicone (ATSO) at a concentration of 2% w/w, and a 60,000 cSt silicone oil; its dynamic viscosity is $\mu_2 = 53 \pm 1 \text{ Pa} \cdot \text{s}$. Hence, in our experiments $\mu_1 \ll \mu_2$. In addition, the SDS in conjunction with the ATSO in the outer liquid result in a low in-

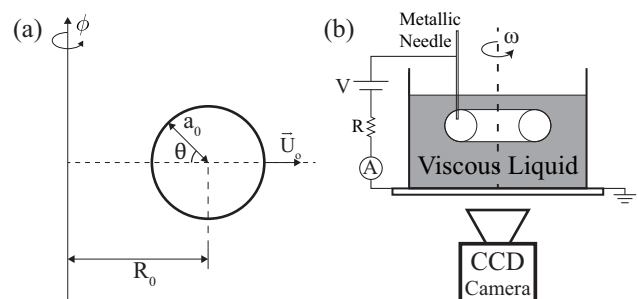


FIG. 1. (a) Schematic of the circular cross section of a torus. R_0 is the radius of the central circle, a_0 is the tube radius, and θ is the polar angle. The torus is obtained by revolving this cross section along the $\hat{\phi}$ direction. The velocity at $\theta = \pi$ is \vec{U}_o . (b) Schematic of the experimental setup. A bath containing silicone oil rotates with an angular speed $\omega \approx 0.25 \text{ rad/s}$ while the inner liquid is injected. The resultant toroidal droplet is charged at a voltage $V \in [0, 1800] \text{ V}$. The subsequent evolution of the torus is captured using a CCD camera.

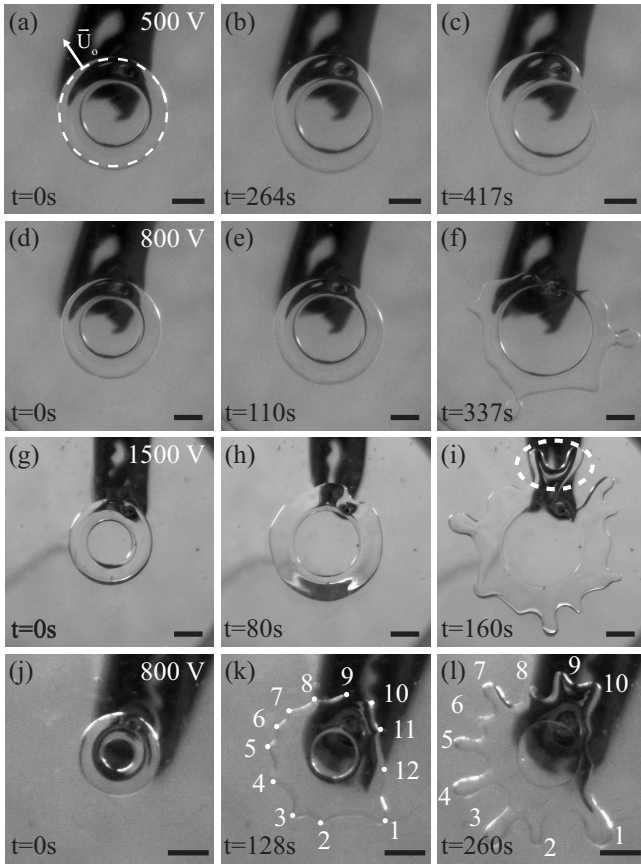


FIG. 2. Snapshots of the evolution of (a-c) a breaking torus with $R_0/a_0 = 3.5$ and $V = 500$ V, (d-f) a torus with $R_0/a_0 = 3.7$ and $V = 800$ V where both break-up and viscous fingering are at play, and (g-i) a torus with $R_0/a_0 = 3.2$ and $V = 1500$ V that clearly exhibits viscus fingering. The dashed circle in (a) represents the outer rim of the torus at $t=0$. The snapshots (j-l) illustrate that some of the initial perturbations do not develop into fingers. The torus has $R_0/a_0 = 2.0$ and the applied voltage is $V = 800$ V. In (k) and (l), we identify with numbers the initial perturbations and the number of fingers at a late stage of development. Scale bars: 2mm.

terfacial tension, which significantly slows down the break-up dynamics; we measure a value of $\gamma = (3.0 \pm 0.5) \cdot 10^{-4}$ N/m using the pendant drop method [7].

For low enough voltage the torus either shrinks and coalesces onto itself to become a single spherical droplet [6, 8–10], or expands before breaking due to Rayleigh-Plateau instabilities [3]; an example of the latter is shown in Fig. 2(a-c) for a torus with an aspect ratio $\xi = R_0/a_0 \approx 3.5$ and at $V = 500$ V. For a similar torus at $V = 800$ V, we observe that the interface slightly distorts, eventually resulting in the formation of fingers; this evolution is exemplified in Fig. 2(d-f). At an even higher voltage of $V = 1500$ V, the interface clearly develops initial perturbations in the outer part of the torus, which evolve into a large number of fingers, as shown in Fig. 2(g-i). We note that it is not uncommon to observe that some of the initial perturbations do not grow at later stages. This is observed at places that can be far or close to the needle, and that

are different for different tori. Hence, despite the fact that the needle could have some local effects in the evolution of the torus, we believe the disappearance of fingers is most likely due to volume conservation. In contrast to experiments with Hele-Shaw cells, where the inner liquid is constantly pumped, our tori contain a fixed volume. As a result, when some of the fingers grow, they consume the available liquid, undermining the growth of nearby fingers; an example of this is shown in Fig. 2(j-l). We also note that individual fingers can divide into two fingers, consistent with what is observed in radial Hele-Shaw cell experiments [11] and as highlighted using a dashed circle in Fig. 2(i); this is also observed at places that could be close or far from the needle, suggesting once again, that even if the needle can induce local perturbations, it does not affect the overall evolution of the torus. We note, however, that finger division is not frequently observed; we believe this is again due to volume conservation. Note that the shadow seen in all images in Fig. 2 is due to the alligator clip used to maintain the metallic needle in place.

We find that the torus expands faster the higher the applied voltage; this can be seen by visually inspecting Figs. 2(b,e,h) and suggests that the speed of expansion affects the appearance of fingers. To determine what sets the expansion speed, we consider the normal stress balance at the interface, which is given by: $p(\theta) - p_o = 2\gamma H - \frac{1}{2}\epsilon E^2$, where $p(\theta) - p_o$ is the pressure jump at the interface, with $p(\theta)$ and p_o the pressures inside the torus at a polar angle θ and outside the torus, respectively, H is the mean curvature, ϵ is the dielectric constant of the outer medium and E is the electric field at the interface. Here, we assume that the torus is a perfect conductor with zero electric field inside and a field perpendicular to the interface on the outside; this is justified given the low electrical relaxation time (≈ 7.1 ns) compared to the typical time scale associated to the toroidal drop evolution. For a torus, $H = \frac{1}{2a_o} \frac{\xi - 2\cos\theta}{\xi - \cos\theta}$ [8], and we use $\epsilon = (3.7 \pm 0.5)\epsilon_o$, with ϵ_o the vacuum permittivity [3]. The field E is calculated analytically [12]. Using this information, we can estimate the pressure difference $\Delta p = p(\theta = 0) - p(\theta = \pi)$ along the expansion direction. Interestingly, Δp determines U_o . We arrive at this result by estimating the viscous stress exerted on a torus from the drag force exerted on a finite cylinder with an aspect ratio ξ_c moving at a speed U_o and oriented perpendicular to the flow direction, and inside a liquid with viscosity μ_2 [13]: $\tau_\mu = \frac{2\pi\mu_2 U_o}{a \ln(0.83\xi_c)}$, where a is the radius of the circular cross section of the cylinder. In our case, we take $\xi_c = \xi$ and $a = a_o$, and obtain that τ_μ is linear with Δp , as shown in Fig. 3, confirming that the expansion speed, for a torus with a given geometry inside a given outer liquid, can be controlled with Δp , and thus with V .

The applied voltage then affects U_o and thus the time scale associated to the observation of viscous fingering. If break-up happens before this instability can develop, however, no fingers are observed. To confirm this, we consider the relevant time scales in either case. For break-up, which is essentially due to Rayleigh-Plateau instabilities, we take $t_{R-P} = \frac{2\mu_2 a_o}{\gamma}$, where the prefactor 2 is obtained for the case of $\mu_1/\mu_2 \ll <$

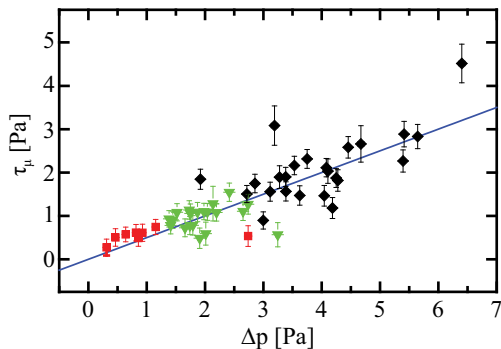


FIG. 3. Viscous stress, τ_μ , as a function of the pressure difference $\Delta p = p(\theta = 0) - p(\theta = \pi)$. (■) Expanding tori that break, (◆) tori that evolve via viscous fingering instabilities, and (▼) tori that exhibit both breaking and viscous fingering. The error bars are calculated by propagating the errors in a_0 , ξ , and U_o , which mostly result from the pixel size of our CCD camera. The line corresponds to a linear fit of the data going through the origin: $\tau_\mu = m \Delta p$, with $m = 0.49 \pm 0.10$.

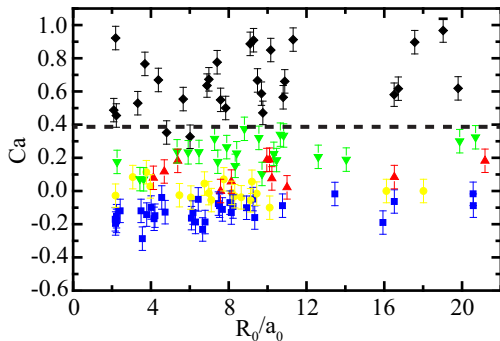


FIG. 4. State diagram in terms of the capillary number Ca and the aspect ratio R_0/a_0 . The symbols represent (■) shrinking tori, (●) tori with stationary central-circle radius, (▲) expanding tori that break, (◆) tori evolving via viscous fingering, and (▼) tori that exhibit both breaking and viscous fingering. The dashed line represents the critical capillary number where only viscous fingering is observed.

1 [15, 16]. For the Saffman-Taylor instability, the relevant time scale is $t_{S-T} = \frac{a_0}{U_o}$ [17], corresponding to the time for the interface of the torus to move its tube radius. Hence, we expect the transition from break-up to viscous fingering will occur when:

$$t_{S-T} < t_{R-P} \Rightarrow Ca = \frac{\mu_2 U_o}{\gamma} > 0.5 \quad (1)$$

where Ca is a capillary number. Experimentally, we observe the clear development of fingers for $Ca \gtrsim 0.4$, as shown in Fig. 4 with a dashed line and consistent with our expectations.

To further support that the instability we observe is related to viscous fingering, we consider the fastest growing mode obtained in a linear stability analysis of the radial Hele-Shaw cell [17]. The basic equation that describes the velocity in this

problem is Darcy's law:

$$\vec{u} = -\frac{b^2}{12\mu} \nabla p, \quad (2)$$

where b is the plate-plate separation, μ is the viscosity of the liquid and p is the pressure. The base solution of the problem is obtained by solving equation 2 for the velocities of both inner and outer liquids, u_{inner} and u_{outer} , respectively, for an unperturbed interface. The boundary conditions at the interface are: $u_{inner} = u_{outer}$ and $p_{inner} - p_{outer} = 2\gamma H$, which correspond to the kinematic boundary condition and the normal stress balance, respectively. The base solution is then sinusoidally perturbed using a number n of wavelengths, as illustrated in the inset in Fig. 5 for $n = 6$; the value of n determines the number of fingers that develop and corresponds to the different modes in the problem. By solving for the perturbed velocity using equation 2, subjected to the same boundary conditions, the growth rate for each n can be calculated [17]. We consider the mode that grows the fastest, as this is the n most likely seen experimentally; it is given by [17, 18]:

$$n_m = \left(\frac{1}{3} \left(\frac{12\mu_2}{\gamma} \frac{UR^2}{b^2} + 1 \right) \right)^{\frac{1}{2}} \quad (3)$$

where U is the velocity of the interface, and R the radius of the stable circle before any fingers develop. To compare with our experimental results, we consider $U = U_o$, $R = R_0 + a_0$ and $b = 2a_0$. Since the theory is a linear stability analysis, the validity of the result is restricted to the early stages of the instability, where the perturbations are still small. We therefore measure n_m right after the perturbations in the outer part of the torus become apparent [see Fig. 2(k)], and plot n_m as a function of $U_o [(\xi + 1)/2]^2$, where we recall that $\xi = R_0/a_0$. We find that the number of fingers grows as $U_o [(\xi + 1)/2]^2$ increases, as shown in Fig. 5 and consistent with what is expected from equation 3. By performing a non-linear least squares fit of the data to equation $n_m = \sqrt{\frac{1}{3} (A U_o [(\xi + 1)/2]^2 + B)}$, where A and B are fitting parameters, we obtain $A = (6.2 \pm 0.2) \cdot 10^6$ s/m and $B = 190 \pm 70$. The fit correctly describes the data, as shown with a continuous line in Fig. 5, indicating that our results conform to the functional form prescribed by equation 3. Furthermore, from the values of μ_2 and γ in our experiments, we find $A = \frac{12\mu_2}{\gamma} = (2.1 \pm 0.3) \cdot 10^6$ s/m, which is comparable to the value of A obtained from the fit. Note, however, that the error in B is large, reflecting our inability to conclude anything meaningful from the behavior of n_m for low $U_o [(\xi + 1)/2]^2$. Indeed, enforcing $B = 1$ and leaving A as the only fitting parameter, still qualitatively describes the data, as shown with a dashed line in Fig. 5, with $A = (8.3 \pm 0.6) \cdot 10^6$ s/m, which is not far from our previous result.

Thus, our data conforms to the functional form prescribed by equation 3 despite the different geometry in our problem and the fact that we did not explicitly account for the presence of charge on the toroidal surface. This suggests that the key to our results is the quasi-two dimensional flow that results from

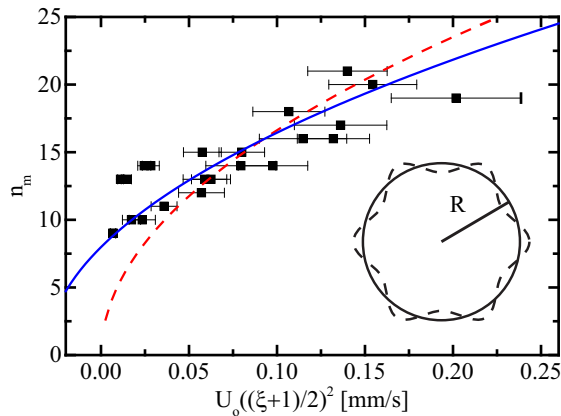


FIG. 5. Number of perturbations, n_m , in the early stages of evolution [see Fig. 2(k)], as a function of $U_o [(\xi + 1)/2]^2$. The continuous and dashed lines are fits to the data (see text). Inset: Top-view schematic of the unperturbed circular interface with radius R (continuous line) and a sinusoidally perturbed interface for $n = 6$ (dashed line).

the uneven charge density distribution on the torus, further supporting the idea that the main role of the charge is to set the value of U_o , which is ultimately the quantity that enters in the theoretical treatment of the radial Hele-Shaw cell. However, explicitly performing the linear stability analysis of the full problem, considering both the presence of surface charge and the toroidal geometry of our experiments, would provide a more accurate analysis of the experimental situation. Our analysis, nevertheless, captures the essential aspects of our observations.

We have shown that the geometry of a charged toroidal droplet can result in a steady quasi-two dimensional expansion that precedes the formation of viscous fingering. This illustrates that it is possible for Saffman-Taylor instabilities, which most commonly occur in confined flows when a fluid displaces another more viscous fluid, can develop in a three-dimensional setting; this had been numerically and theoretically proposed before in a different context [19]. In our experiments, it is the uneven surface charge distribution between the inside and outside regions of the torus that ultimately enables the formation of fingers. This instability is in direct competition with the Rayleigh-Plateau instability, which would cause the torus to break. As a result, the instability that grows fastest is the one that determines the fate of the toroidal drop. By controlling the expansion speed with the applied voltage, we are able to decrease the time scale associated to viscous fingering so that it is this instability that controls the evolution of the

torus. The number of fingers in the experiments qualitatively follows the expected number of fingers obtained from linear stability analysis in radial Hele-Shaw cells, supporting that our observations are related to Saffman-Taylor instabilities. However, more detailed theoretical calculations are needed to fully obtain a detailed picture of the problem. Most importantly, the breaking of axisymmetry in a torus is key to our observations, suggesting that similar behavior is also possible in situations where due to the three-dimensional character of the flows, viscous fingering would not be anticipated. This could potentially extend the relevance of this instability to situations other than two phase flows in porous media, which is perhaps where it is of most importance.

We thank financial support from the National Science Foundation. We also thank Irmgard Bischofberger for useful comments and suggestions.

-
- [1] R. Osserman, *Bull. Am. Math. Soc.* **84**, 1182 (1978).
 - [2] G. I. Taylor, *Proc. R. Soc. A* **280**, 383 (1964).
 - [3] A. A. Fragkopoulos, A. Fernandez-Nieves, *Phys. Rev. E* **95**, 033122 (2017).
 - [4] P. G. Saffman, G. I. Taylor, *Proc. R. Soc. A* **245**, 312 (1958).
 - [5] I. Bischofberger, R. Ramachandran, S. R. Nagel, *Nature Commun.* **5**, 5265 (2014).
 - [6] E. Páram, A. Fernández-Nieves, *Phys. Rev. Lett.* **102**, 234501 (2009).
 - [7] C.E. Stauffer, *J. Phys. Chem.* **69**, 1933 (1965).
 - [8] Z. Yao, M. J. Bowick, *Eur. Phys. J. E Soft Matter* **34**, 1 (2006).
 - [9] M. Zabarankin, O. M. Lavrenteva, A. Nir, *J. Fluid Mech.* **785**, 372 (2015).
 - [10] A. A. Fragkopoulos, E. Páram, E. Berger, P. N. Segre, A. Fernandez-Nieves, *Proc. Nat. Acad. Sci.* **114**, 2871 (2017).
 - [11] I. Bischofberger, R. Ramachandran, S. Nagel, *Soft Matter* **11**, 7428 (2015).
 - [12] J.A. Hernandez, A.K.T. Assis, *Phys. Rev. E* **68**, 046611 (2003).
 - [13] H. A. Stone, *J. Fluid Mech.* **645**, 1 (2010).
 - [14] G. K. Batchelor, Cambridge Univ Press, Cambridge, UK (1967).
 - [15] S. Tomotika, *Proc. R. Soc. A* **150**, 322 (1935).
 - [16] We note that for the aspect ratios and voltages in our experiments, the presence of surface charge does not appreciably affect the growth rate of the fastest unstable mode; see Q. Wang, D. T. Papageorgiou, *J. Fluid Mech.*, **683**, 27 (2011).
 - [17] L. Paterson, *J. Fluid Mech.* **113**, 513 (1981).
 - [18] A. Buka, P. Pálffy-Muhoray, Z. Racz, *Phys. Rev. A* **36**, 3984 (1987).
 - [19] H. Levine, Y. Tu, *Phys. Rev. A* **45**, 1044 (1992).